Paper A

Can dawsonite permanently trap CO_2?

Hellevang, H.
Aagaard, P.
Oelkers, E.H.
Kvamme, B.

Published in Environmental *Science and Technology*, 2005, **39**, 8281-8287

Can Dawsonite Permanently Trap CO_2?

HELGE HELLEVANG,[†] PER AAGAARD,*[,‡] ERIC H. OELKERS,[§] AND BJØRN KVAMME[†]

Department of Physics and Technology, University of Bergen, Allégt. 55, 5009 Bergen, Norway, Department of Geoscience, University of Oslo, P.B. 1047 Blindern, 0316 Oslo, Norway, and Géochimie et Biogéochimie Experiméntale, LMTG, Université Paul Sabatier/CNRS-UMR 5563, 14 rue Ave Edouard Belin, 31400 Toulouse, France

Thermodynamic calculations indicate that although dawsonite ($NaAlCO_3(OH)_2$) is favored to form at the high CO_2 pressures associated with carbon dioxide injection into sandstone reservoirs, this mineral will become unstable as CO_2 pressure decreases following injection. To assess the degree to which dawsonite will persist following its formation in sandstone reservoirs, its dissolution rates have been measured at 80 ± 3 °C as a function of pH from 3 to 10. Measured dawsonite dissolution rates normalized to their BET surface area are found to be nearly independent of pH over the range of 3.5 < pH < 8.6 at 1.58×10^{-9} mol/(m^2•s). Use of these dissolution rates in reactive transport calculations indicate that dawsonite rapidly dissolves following the decrease of CO_2 pressure out of its stability field, leading mainly to the precipitation of secondary kaolinite. This result indicates that dawsonite will provide a permanent mineral storage host only in systems that maintain high CO_2 pressures, whereas dawsonite may be an ephemeral phase in dynamic settings and dissolve once high CO_2 pressure dissipates either through dispersion or leakage.

Introduction

Increasing atmospheric concentrations of greenhouse gases are expected to cause a gradual warming of the Earth's surface, leading to potentially disastrous global climate changes. Because carbon dioxide is a major greenhouse gas, different strategies have been suggested to limit its concentration in the atmosphere. One option is the injection of CO_2 into geologic formations (*1*−*4*). Once CO_2 is injected, it will migrate as an immiscible gas or supercritical fluid, and accumulate beneath impermeable structures. Limited by temperature, pressure, and salinity, it will gradually dissolve into the aqueous solution, and react to form carbonic acid, and bicarbonate and carbonate ions. Increased acidity induces dissolution of primary minerals, and subsequent neutralization leads to precipitation of secondary phases, including carbonates. Such secondary carbonates are commonly viewed as a permanent host for injected CO_2.

Owing to the abundance of aluminosilicate minerals in sedimentary rocks, one secondary carbonate that is predicted to precipitate as a reaction product in sequestering simulations, is dawsonite ($NaAlCO_3(OH)_2$; e.g., refs *5*−*8*). The simulations commonly show a steady growth of dawsonite and other carbonates such as calcite, magnesite, siderite, and ankerite coupled to aluminosilicate dissolution at elevated CO_2 pressures. Simulations by Xu et al. (*8*) suggest that dawsonite precipitates as a dominant CO_2 bearing phase in divalent-cation-poor sandstones and as a subordinate phase compared to other carbonates in glauconitic sandstones and ultramafic rocks. Simulations also suggest that although the volume fraction of CO_2 stored as solid carbonate may be limited at short time scales (<1000 years), it may have a major role in preventing the CO_2 escape to the surface (*5*).

Precipitation of dawsonite is also supported by field observations. For example large volumes of dawsonite have been observed in the oil shales in the Green River Formation (*9*); natural occurrences of dawsonite have also been linked to CO_2 seepage into groundwater (*10*). These occurrences are linked, however, to alkaline or highly alkaline solutions, and dawsonite is a rare mineral in nonalkaline systems. For example, Pearce et al. (*11*) reported that the rocks of the Bravo Dome natural CO_2 field in New Mexico are extensively corroded due to their interaction with CO_2-charged acidified waters. Dawsonite precipitation, however, was not observed in this system. Such observations suggest that if dawsonite does precipitate at nonalkaline conditions it is only an ephemeral phase which decomposes when CO_2 pressure drops. Once dawsonite is destabilized, it will dissolve at a rate determined by the dissolution and precipitation kinetics of the minerals that constitute the system. Since dawsonite dissolution rates have yet to be reported in the literature, sequestering simulations have used a variety of methods to estimate these rates. For example, Gaus et al. (*7*) assumed that dawsonite dissolution rates are intermediate between that of calcite and dolomite, whereas Xu et al., (*8*) assumed that dawsonite dissolution rates are equal to that of K-feldspar.

This study is motivated by the need to better understand the potential role of dawsonite in CO_2 storage scenarios. Toward this goal, dawsonite dissolution rates have been measured as a function of pH from 3 to 10 at 80 ± 3 °C. These rates have been used together with dissolution/precipitation rates of other minerals obtained from the literature to assess the long-term stability of dawsonite in sedimentary basins as a function of the partial pressure of CO_2. The aim of this paper is (1) to report the results of this combined experimental and computational study and (2) to better define what role dawsonite may play in geologic storage of CO_2.

Theoretical Background

Dawsonite dissolution and precipitation can be described using

$$NaAlCO_3(OH)_2 + 4H^+ \rightarrow Na^+ + Al^{3+} + CO_{2(aq)} + 3H_2O \quad (1)$$

Dawsonite stability is, therefore, strongly related to aqueous CO_2 concentration, which itself can be related to the partial pressure of a coexisting CO_2 phase by taking account of

$$CO_{2(g/fl)} \leftrightarrow CO_{2(aq)} \quad (2)$$

where subscripts (g/fl) and (aq) refer to CO_2 as gas/fluid

* Corresponding author phone: (0047)22856644; fax: (0047)-22854215; e-mail: aagaard@geo.uio.no.
† University of Bergen.
‡ University of Oslo.
§ Université Paul Sabatier.

10.1021/es0504791 CCC: $30.25
Published on Web 09/21/2005

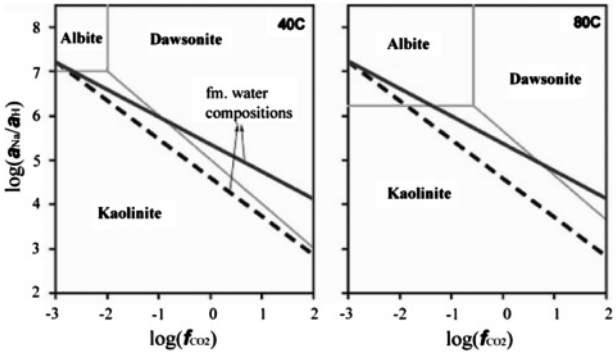

FIGURE 1. Log fugacity−activity diagram depicting mineral stability fields in the system $Na_2O-Al_2O_3-SiO_2-CO_2-H_2O$ at 40 and 80 °C. The dashed and solid lines represent different formation water compositions. The dashed line was computed by equilibrating the formation water with varying CO_2 fugacities, whereas the solid line was computed by equilibrating seawater simultaneously with calcite, acting as a pH buffer, and varying CO_2 fugacities.

phase and aqueous phase, respectively. The law of mass action for reaction 2 is given by

$$K_H = \frac{a_{CO2}}{f_{CO2}} \quad (3)$$

where a_i and f_i denote the activity and fugacity of the subscripted species, and K_H refers to the Henry's law coefficient, which is provided together with its temperature dependence in the LLNL thermodynamic database.

The relative stability of dawsonite with respect to other Na and Al bearing phases can be assessed using logarithmic activity−fugacity diagrams such as those illustrated in Figure 1. The activity diagrams presented in this figure illustrate phase relations in the system $Na_2O-Al_2O_3-SiO_2-CO_2-H_2O$ balanced on aluminum with SiO_2 activity fixed by quartz saturation. The solid lines in this activity diagram represent fluid compositions in equilibrium with the two minerals adjoining these lines and are computed from the law of mass action for reactions among these minerals. For example, equilibrium between albite and dawsonite can be represented by

$$NaAlSi_3O_8 + H_2O + CO_{2(aq)} \leftrightarrow NaAl(OH)_2CO_3 + 3SiO_{2(aq)} \quad (4)$$

Rearranging the law of mass action of reaction 4 yields

$$\log(f_{CO2}) = \log\left(\frac{K_{e4}a_{SiO2}^{\ 3}}{K_H}\right) \quad (5)$$

where K_H and K_{e4} designate the Henry's law constant for CO_2 and the equilibrium constant for reaction 4 respectively.

Dawsonite stability increases with increasing a_{Na+}/a_{H+} and f_{CO2}, but decreases with increasing temperature. Two representative fluid composition paths are traced in this figure. The first is shown as a dashed line and corresponds to the composition of seawater equilibrated with varying fugacities of CO_2. Dawsonite is not stable in this fluid at any temperature above 40 °C and a CO_2 fugacity below 100, corresponding to a CO_2 partial pressure of approximately 185 bar. The solid line in Figure 1 corresponds to the composition of seawater equilibrated simultaneously with varying fugacities of CO_2 and calcite according to

$$CaCO_3 + CO_{2(aq)} + H_2O \rightarrow Ca^{2+} + 2HCO_3^- \quad (6)$$

Increasing CO_2 fugacity in this system leads to calcite dissolution and consumption of some aqueous CO_2. At 40 °C, dawsonite is stable in this fluid at all CO_2 fugacities greater than 0.1. At higher temperatures, higher CO_2 fugacities are required to stabilize dawsonite. At 80 °C, dawsonite stability requires a CO_2 fugacity of approximately 6.3, corresponding to a partial pressure of 10 bar. The stability of dawsonite at elevated CO_2 pressures has led numerous scientists to propose dawsonite as a potential long-term CO_2 storage host, particularly in divalent-cation-poor sedimentary basins. In contrast, as injected CO_2 gas disperses, dissolves in, or leaks from the sequestrating formation following its injection, CO_2 fugacity would decrease, potentially destabilizing dawsonite relative to aluminosilicate phases. The degree to which dawsonite would persist in response to decreases in CO_2 partial pressure can be assessed from comprehensive geochemical modeling calculations if dawsonite dissolution rates are known. Such rates were determined in the present study as described below.

Materials and Methods

Starting Material. Natural dawsonite specimens were obtained from Monticolo, Terlano, Alto Adige in Italy. This dawsonite occurs as white fibrous or massive material in vugs and fractures. Its fibrous habit and color contrast relative to the surrounding mineral phases facilitated dawsonite extraction from the host rock. Two growth habits, massive and fibrous, were separated for X-ray diffraction (XRD) analysis. XRD analysis of the ground samples showed both the fibrous and massive material to be pure dawsonite with less than 1% impurities. The massive and fibrous materials were subsequently mixed and homogenized. Because of its fragile nature and small crystal size, attempts to ultrasonically clean this material were unsuccessful. To remove the relatively fine particles, therefore, 10% of the dawsonite powder was dissolved in each experiment prior to rate measurement. The specific surface area of the dawsonite powder, prior to the experiments, was determined to be 11.54 m^2/g, using the BET technique with N_2 adsorption.

Thermodynamic Calculations. The standard state adopted in this study is that of unit activity for pure minerals and H_2O at any temperature and pressure. For aqueous species other than H_2O, the standard state is unit activity of the species in a hypothetical 1 molal solution referenced to infinite dilution at any temperature and pressure. For gases, the standard state is for unit fugacity of a hypothetical ideal gas at 1 bar of pressure. All thermodynamic calculations were performed using the geochemical code PHREEQC-v2 (*12*) together with the thermo.com.V8.R6.230 thermodynamic database compiled at Lawrence Livermore National Laboratory. Activities of charged aqueous species are calculated according to the "b-dot" equation (*13*), whereas the fugacity of CO_2 is computed as a function of temperature and pressure using the SRK equation of state (*14*) together with algorithms reported by Mollerup and Michelsen (*15*).

Experimental and Analytical Procedures. All dawsonite dissolution rate experiments reported in the present study were performed in 250 mL polyethylene Azalon beakers covered with a fitted Teflon cover. This cover had several holes allowing continuous contact between the reactive fluid and atmospheric CO_2. Experiments were initiated by placing 0.2 to 0.5 g of dawsonite powder in the reactor and adding from 150 to 190 g of initial reactive fluid. Reactive fluids having an initial pH from 2 to 9.4 were composed of demineralized/deionized H_2O (e.g., experiment DD-3) plus either Merck analytic grade HCl (e.g., experiments DD-1, 2, 4, 6, and 7) or a mixture of NH_4OH and NH_4Cl (e.g., experiment DD-5). These batch reactors were placed in a constant temperature (80 °C) shaker bath to ensure fluid mixing and to avoid dawsonite powder grinding. Four to five milliliters of reactive solution was sampled regularly using syringes equipped with

TABLE 1. Summary of Experimental Results[a]

expt no.	elapsed time (s)	V (L)[b]	pH_{80}[c]	C_{Na} (mg/l)	C_{Al} (mg/l)	m_i (g)[d]	m_i/m_0	SI_{daws}[e]	log(r) (mol/m^{2}s)
DD-1 PRE	100890 0	0.146	3.89	7.505	7.226	0.0206	0.75		
DD-1-1	56700	0.134	3.70	10.85	6.12	0.0154	0.60	−5.72	−8.437
DD-1-2	92340	0.127	3.74	11.34	6.09	0.0150	0.59	−5.61	−9.334
DD-2 PRE	602580	0.147	4.33	0.71	bdl[f]	0.0714	0.99		
DD-2-1	55920	0.145	7.76	12.23	0.2	0.0602	0.84	−4.3	−8.710
DD-2-2	92640	0.136	7.76	17.94	0.47	0.0550	0.77	−3.77	−8.814
DD-2-3	177000	0.127	7.81	23.55	2.21	0.0503	0.70	−2.98	−9.178
DD-2-4	228960	0.117	7.85	25.61	2.45	0.0486	0.68	−2.9	−9.402
DD-2-5	265500	0.108	7.9	28.08	1.91	0.0468	0.65	−2.97	−9.167
DD-2-6	315000	0.099	7.94	31.78	0.27	0.0443	0.61	−3.77	−9.112
DD-2-7	347640	0.089	7.98	33.22	0.48	0.0434	0.60	−3.5	−9.349
DD-3-1	18180	0.163	6.83	4.39	0.07	0.0295	0.87	−5.79	−8.360
DD-3-2	69180	0.155	6.92	13.77	0.39	0.0204	0.60	−4.78	−8.364
DD-4 PRE	18180	0.177	4.06	71.66		0.724	0.90		
DD-4-1	102180	0.169	5.43	187.49	0.19	0.601	0.75	−4.89	−8.888
DD-4-2	162180	0.161	7.10	211.42	0.29	0.577	0.72	−2.97	−9.432
DD-4-3	240240	0.224	5.79	189.38	0.73	0.504	0.63	−3.31	−9.019
DD-4-4	272520	0.236	3.53	176.54	4.39	0.491	0.61	−8.07	−9.365
DD-5-1	13800	0.178	8.65	5.17	0.19	0.0288	0.83	−4.73	−8.140
DD-6 PRE	4800	0.148	6.11	0.65966		0.00932	0.9508		
DD-6-1	24840	0.138	7.54	4.15	0.29	0.00721	0.74	−4.6	−8.168
DD-7 PRE	1800	0.128	3.979	1.1290		0.00889	0.9074		
DD-7-1	5400	0.12	4.23	2.01	0.14	0.00823	0.84	−7.02	−7.903
DD-7-2	21540	0.112	5.5	3.78	0.15	0.00698	0.71	−4.94	−8.249
DD-7-3	41100	0.104	5.72	4.42	0.22	0.00656	0.67	−4.7	−8.734
DD-7-4	79680	0.096	5.92	5.42	0.1	0.00596	0.61	−4.94	−8.842

[a] To avoid fine particle dissolution, approximately 10% of the dawsonite mass was dissolved prior to dissolution rate measurement. Experiments labeled (DD-*x* PRE*)* refer to the reactor conditions at the end of this pretreatment procedure. Experiments are labeled in the sequential order of their measurement. The experiments were stopped as soon as 40% of the initial material had dissolved. [b] Volume in reactor prior to sampling, except for the pretreatment procedure where the initial volume is provided. [c] pH measured at 25 °C and recalculated to 80 °C. [d] Mass of dawsonite present in reactor prior to sampling. [e] SI = log(Q/K), where K is the equilibrium constant for dawsonite dissociation and Q is the ion activity product for the reaction. The solubility indices are calculated with PHREEQC v2 from solution compositions measured at 25° C and assuming these solutions are in equilibrium with atmospheric CO_2 pressure. [f] bdl, below detection limit.

0.45 μm micropore filters. Additional initial solution was added after the second (DD-4−2) and third (DD-4−3) sampling of experiment DD-4 (Table 1), to avoid the reactive solution attaining dawsonite equilibrium. Powder pretreatment was performed by dissolving 10% of the initial dawsonite in the same reactive fluid as that used in the subsequent dissolution experiment. This pretreatment was monitored by regular reactive fluid sampling and analysis. Additional initial reactive fluid was added to the reactor at the end of the pretreatment and prior to dissolution rate measurement.

Aqueous sodium and aluminum analyses were performed using a Perkin-Elmer 5100 atomic absorption spectrophotometer. The uncertainties associated with these measurements are estimated to be ±5%. Reactive solution pH was measured at 25° C within a few hours of sampling using a Metrohm 744 pH meter coupled to a calibrated Metrohm Pt1000/B/2 electrode with a 3 M KCl outer filling solution. Uncertainty of these measurements is estimated to be ±0.05 pH units.

Rate Measurements. Distinct dissolution rates were computed from each reactive solution sampled obtained during the experiments. These rates are generated from the change of aqueous Na concentrations as a function of time using

$$r_{t\rightarrow t+1} = \frac{1}{s\nu m_{t\rightarrow t+1}} \frac{\Delta n_{t\rightarrow t+1}}{\Delta t} \quad (7)$$

where $r_{t\rightarrow t+1}$ refers to the average dawsonite dissolution rate determined from the measured reactive fluid *sodium* concentrations from time t to $t+1$, s stands for the specific BET surface area of the initial dawsonite powder, ν designates the stoichiometric number of moles of *sodium* in one mole of dawsonite, $m_{t\rightarrow t+1}$ denotes the average mass of dawsonite present in the reactor at time t to $t+1$, $\Delta n_{t\rightarrow t+1}$ represents the change in the molar mass of sodium present in the reactive solution from t to $t+1$, Δt corresponds to the elapsed time between t and $t+1$. The mass of dawsonite present in the reactor was calculated from mass balance calculations in accord with

$$m_t = m^0 - M\sum_{t=0}^{t} \Delta n_{\mathrm{Na},t\rightarrow t+1} \quad (8)$$

where m^0 represents the initial mass of dawsonite present in the reactor and M stands for the molar mass of dawsonite (144.0 g/mol). Note that rates in the present study were computed using the specific BET surface area of the initial dawsonite powder. Insufficient powder was recovered from each experiment to measure the specific BET surface areas of the postexperiment dawsonite powders.

Geochemical Modeling . Reactive transport calculations were performed in the present study using the PHREEQC-2 geochemical code. A postinjection scenario consisting of an injection site with a slow regional flow of formation water (0.1m/y) was considered. This system was modeled using a single 1D column that crosses horizontally through 10 m of this injection site. The site is assumed to consist of the simplified mineralogy listed in Table 2. The pore fluids in

TABLE 2. Initial Mineral Abundances, Porosity, Radius of Uniform Spherical Grains, Calculated Initial Interfacial Surface Areas, and Apparent Activation Energies Used in the Reactive Transport Calculations

mineral	vol %	r (mm)[a]	A (m^2/ dm^3)[b]	k_{80} (mol/m^2s)[c]	E_a (kJ/mol)	ref
quartz	55.7	0.3	222.8	3.07×10^{-12}	87.50	29
albite	10.0	0.3	40.0	7.09×10^{-11}	67.83	30
kaolinite	3.0	0.005	720.0	2.05×10^{-11}	62.76	31
dawsonite	0.3	0.07	5.0	1.58×10^{-9}		this study
calcite	6.0	0.3	24.0	2.22×10^{-8}	41.87	32
porosity	25					

[a] Radius of uniform sized spheres; used to calculate the surface area per liter of solution. [b] Interfacial surface areas are calculated using the geometric model described in the text. [c] The kinetic constants given in the table are calculated from 25 ° C data reported in refs *29*−*32*, recalculated to 80 °C using eq 10, except for the dawsonite dissolution kinetics which are measured directly at 80 °C.

TABLE 3. Water Compositions (mol/kg of H_2O) Used for Reactive Transport Calculations[a]

chemical component	solutions		
	i	1	2
Ca^{2+}	3.03×10^{-2}	2.32×10^{-2}	1.22×10^{-2}
Mg^{2+}	1.07×10^{-4}	1.28×10^{-4}	1.28×10^{-4}
Na^{+}	0.946	0.918	0.939
K^{+}	1.75×10^{-2}	1.75×10^{-2}	1.75×10^{-2}
Fe^{2+}	4.07×10^{-8}	1.72×10^{-7}	1.81×10^{-7}
SiO_2(aq)	5.71×10^{-4}	5.71×10^{-4}	5.71×10^{-4}
HCO_3^{-}	5.37×10^{-2}	3.46×10^{-3}	2.69×10^{-3}
Al^{tot}	1.77×10^{-8}	7.00×10^{-8}	1.55×10^{-7}
Cl^{-}	0.968	0.970	0.969
pH	4.754	6.056	6.446

[a] Solution "*i*" is the formation water chemistry for the initial solution at a CO_2 fugacity of 100; solutions 1 and 2 refer to the two inflowing solutions in simulations 1 and 2, respectively. Solution 1 is also used for the dawsonite lifetime calculations.

this system are initially in equilibrium with these minerals and have a CO_2 fugacity of 100 at 80 °C. The composition of this formation water is given in Table 3.

Mineral dissolution and precipitation rates in this calculation are assumed to be consistent with

$$r = k_{80}A\left(1 - \frac{Q}{K}\right) \tag{9}$$

where A represents the mineral/fluid interfacial surface area, Q and K designate the reaction product and equilibrium constants, respectively, for the mineral reaction, and k_{80} stands for the rate constant at 80 °C. Some of these rates are extrapolated from reported rate constants at 25 °C using the Arrhenius relation (see Table 2);

$$k_{80} = k_{25}e^{-Ea/R(1/T\,-\,1/298.15)} \tag{10}$$

where E_a represents the apparent activation energy for the reaction. Keiffer et al. (*28*) showed that simple geometric models can be used to quantify surface areas of sedimentary rocks involved in water-rock reactions. Thus, the interfacial surface area for the different minerals is estimated geometrically assuming that mineral grains are uniform sized spheres; kaolinite and dawsonite radii are assumed to be smaller than other minerals to account for their higher surface areas. The use of a more advanced geometric model including needle and platy habits for dawsonite and kaolinite, respectively, did not significant change the simulation results. Surface roughness is assumed to increase the surface area by 1 order of magnitude for all minerals.

Experimental Results

Dawsonite dissolution rates were measured in unbuffered reactive solutions. As such, the consumption or liberation of protons during dawsonite dissolution leads to a continuous change in reactive solution pH. This pH change is advantageous because it allows rate measurements over a wide range of pH from a limited number of experiments performed using a limited quantity of dawsonite powder.

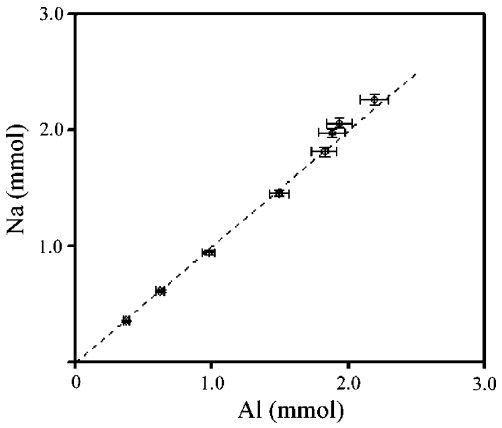

FIGURE 2. Molar concentration of sodium plotted as a function of the molar concentration of aluminum in all gibbsite undersaturated reactive solutions. The dashed line corresponds to a 1:1 slope consistent with stoichiometric dawsonite dissolution. Error bars indicate 2% and 5% analytical uncertainty for sodium and aluminum, respectively.

The use of eq 7 to compute dawsonite dissolution rates is predicated on the assumption that sodium is released stoichiometrically during the experiments. To assess this assumption, measured solution sodium concentrations in all reactive solutions that were undersaturated with respect to gibbsite are plotted as a function of the corresponding aluminum concentration in Figure 2. The dashed line in this figure corresponds to equal sodium and aluminum concentrations, which is consistent with stiochiometric dawsonite dissolution. The close correspondence between the symbols and the dashed line in Figure 2 suggests that (1) dawsonite dissolution was stoichiometric and (2) the dawsonite used in this study is consistent with the formula $NaAlCO_3(OH_2)$. All reactive solutions at pH > 3.5 were supersaturated with respect to gibbsite but undersaturated with respect to sodium-bearing phases. As a result, the molar concentrations of aluminum in these reactive solutions were less than that of sodium. Consequently, it is assumed that at pH > 3.5, reactive fluid sodium concentrations stem solely from dawsonite dissolution, whereas corresponding aluminum concentrations reflect the combined affects of dawsonite dissolution and gibbsite precipitation.

Far-from-equilibrium dawsonite dissolution rates and the compositions of all reactive solutions are listed in Table 1 and illustrated as a function of pH in Figure 3. The bold line through the symbols represents a rate of 1.58×10^{-9} mol/(m^2·s). The pH at 80 °C of each experiment was calculated

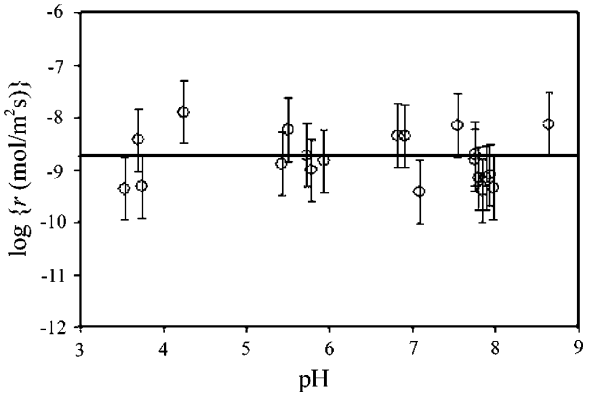

FIGURE 3. Measured far-from-equilibrium dawsonite dissolution rates at 80 °C as a function of pH. The symbols represent measured rates, the error bars correspond to a combined uncertainty of ±0.6 log units, and the bold line represents a constant rate of 1.58 × 10^{-9} mol/m^2·s.

from fluid compositions measured at 25 °C. Results suggest that dawsonite dissolution rates are independent of pH to within analytic uncertainty over the range 3.5 < pH < 8.6. This pH independence of rates is consistent with corresponding observations made on other carbonate minerals. For example, calcite, dolomite, and magnesite dissolution rates at 25 °C are found to be pH independent from ~4.5 < pH < 11 (*16*−22). Dawsonite dissolution rates are lower than corresponding rates of the common carbonates calcite and dolomite; Gauthelier et al. (*23*) reported that the dissolution rate of dolomite at 80 °C and pH ~4.3 is ~6 × 10^{-6} mol/(m^2·s); Alkataan et al. (*24*) report that the dissolution rate of calcite at 80 °C and pH ~3.3 is ~1 × 10^{-4} mol/(m^2·s). In contrast, measured dawsonite dissolution rates are several orders of magnitude faster than the corresponding rates of aluminosilicates. The degree to which the dissolution rate of dawsonite will affect its stability during CO_2 storage scenarios is explored below.

The degree of uncertainty on measured dawsonite dissolution rates is difficult to assess but may be large. One potential contribution to the uncertainty is the changing dawsonite surface area during the experiments. The surface area used to compute rates was that measured on the initial powder. This surface area could change due to preferential dissolution of fine particles and/or gibbsite precipitation on the dawsonite surfaces. Moreover, rates are based on the differences of Na concentrations measured in consecutive reactive solution samples. The use of differences in concentration amplifies the analytic uncertainties in the Na analyses. When these factors are taken into account, along with the scatter apparent on Figure 3, a reasonable estimate of the uncertainty of the rates listed in Table 1 is ±0.6 log units. This uncertainty is equivalent to a factor of ±4. Mineral surface areas have commonly been observed to vary by a factor of 4 or more during laboratory dissolution experiments (cf. *25*, *26*)

Will Dawsonite Persist Long-Term Following the Injection of CO_2 into Sedimentary Rocks? Thermodynamic calculations indicate that dawsonite is stable and likely to precipitate at the elevated CO_2 partial pressures expected during the injection of CO_2 into sedimentary rocks (e.g., refs *5*−*8*). Nevertheless, CO_2 partial pressure in these systems can be expected to drop once CO_2 injection is arrested. The reduction of CO_2 partial pressure is favored in both dynamic and closed hydrodynamic systems. In closed systems, CO_2 partial pressure would drop as CO_2 is dissolved and dispersed in the formation waters with time. More significantly, in open systems, the increased buoyancy and lower viscosity of a free CO_2 phase will make it particularly susceptible to transport both toward the Earth's surface and in the direction of regional fluid flow. A significant drop in CO_2 partial pressure could destabilize dawsonite leading to its dissolution. The degree and rate at which dawsonite dissolves and liberates carbonate to the aqueous phase can be assessed with the aid of reactive transport calculations.

Reactive transport modeling is based on the system described above. Two different NaCl-rich formation waters infiltrate this system at a 0.1 m/y flow rate with Cauchy boundary conditions at both ends. The compositions of these infiltration fluids are listed in Table 3. The first fluid is

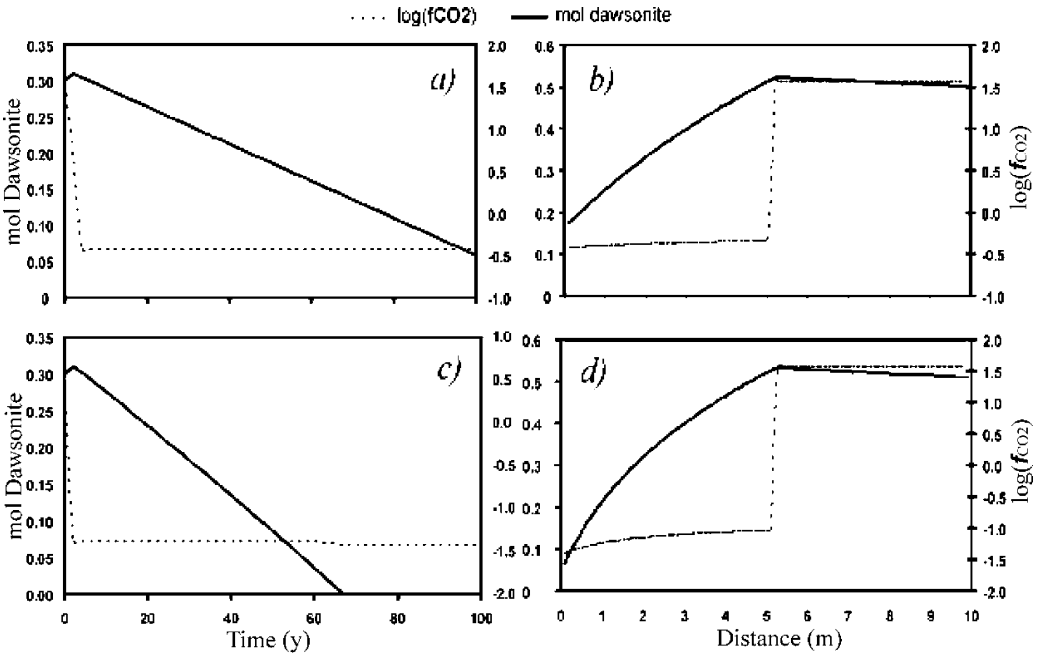

FIGURE 4. Results of postinjection reactive transport simulations: plots a and b illustrate results for the infiltration of solution 1, which is in the kaolinite stability field, whereas plots c and d illustrate results for the infiltration of solution 2, which is in the albite stability field. The compositions of these solutions are listed in Table 3. Plots a and c shows the temporal evolution of dawsonite abundance and pore fluid f_{CO_2} at a distance of 0.2 m from the source of the infiltrating fluids, whereas plots b and d show the spatial abundance of dawsonite and pore fluid f_{CO_2} as a function of distance from the infiltration point, 50 y after the start of formation water infiltration—see text.

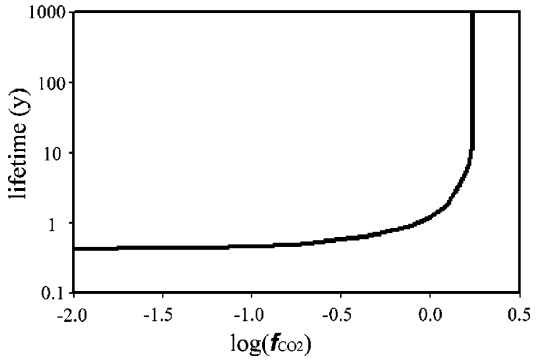

FIGURE 5. Lifetime of a 1 mm dawsonite grain at different CO_2 fugacities. Dawsonite starts to dissolve as soon as the partial pressure of CO_2 drops below the dawsonite stability field. Dissolution accelerates as f_{CO_2} decreases further and dawsonite becomes more undersaturated.

undersaturated with respect to albite ($SI_{alb} = -0.4$). The solution resides in the kaolinite stability field and has a CO_2 pressure of 1 bar, consistent with the CO_2 pressures of typical North Sea formation waters (*27*). The second solution is in the albite stability field and has a CO_2 pressure of $10^{-1.3}$ bar. Both the temporal evolution of mineral abundances at a fixed position in the column and the spatial variation of mineral abundances at a fixed time are computed.

The infiltration of both fluids leads to a drop in CO_2 fugacity, which results in the pore fluid moving into the stability fields of kaolinite and albite, respectively (see Figure 1). This provokes albite and kaolinite precipitation coupled to dawsonite dissolution (i.e., the reverse of eq 4). In the first simulation, less than 20% of the dawsonite persists in the first cells of the column 100 years after termination of CO_2 injection (see Figure 4a). In this case kaolinite precipitates and dawsonite and albite dissolve. The sodium that is added to the fluid phase due to dawsonite and albite dissolution is transported through the column and the fluid approaches equilibrium with kaolinite, albite, and dawsonite near the outlet. Dawsonite thereby dissolves in the first cells of the column and precipitates in cells that follow. Eventually, the inflowing fluid will flush the whole column and dissolve all the dawsonite. In the second case, the inflowing solution is in the albite stability field. The advection of this fluid into the column leads to kaolinite and albite precipitation coupled to dawsonite dissolution (see Figure 4c). Since both dawsonite and albite contain one mol of sodium per mol of mineral, and as albite precipitation is slower than dawsonite dissolution, sodium concentration increases in the pore fluid. Nevertheless, due to kaolinite and albite precipitation, dawsonite dissolves faster in this scenario.

One additional simple calculation was performed to determine the lifetime of dawsonite in undersaturated solutions as a function of CO_2 fugacity. The result of this calculation is illustrated in Figure 5. The degree of dawsonite undersaturation was calculated using the PHREEQC-2 by equilibrating solution 1 (Table 3) with varying CO_2 fugacities. The surface area of the dawsonite was assumed to be equal to that measured in this study, i.e., 11.54 m^2/g. Dawsonite dissolution rates are assumed to vary as a function of chemical affinity according to eq 9. The calculation suggests that dawsonite will persist for only short time periods following a drop of CO_2 pressure from the dawsonite stability field. For example, a 1 mm dawsonite grain is estimated to persist less than one year in a solution having a typical formation water CO_2 fugacity of 1.

The degree to which dawsonite dissolution is detrimental to the long-term storage of CO_2 depends on the fate of the liberated aqueous carbonate species. These species could either form different stable carbonate species or ultimately be exolved and liberated from solution as CO_2 gas or fluid. Most stable carbonate phases are composed of divalent metals such as calcium, magnesium, and iron. The availability of these metals depends on the mineralogy of the system and their reactivity. In general, the mineralogy of typical injection sites is dominated by quartz and divalent-cation-poor aluminosilicate minerals. In such systems it is unlikely that the liberation of carbonate from dawsonite dissolution will provoke the precipitation of significant amounts of other carbonate minerals. Such may not be the case for glauconitic sands and typical gulf coast sediments which have a high abundance of oligoclase (*8*). However, for divalent-cation-poor reservoirs, dawsonite dissolution will provoke a rise in CO_2 fugacity, which could ultimately lead to its exsolution into a separate gas or fluid phase. This phase could be physically trapped in the reservoir, dispersed back into the aqueous phase with time, or in the worst case scenario migrate upward and escape into the atmosphere.

Acknowledgments

We thank J. Schott, O. Pokrovsky, P. Benezeth, and S. Callahan for helpful discussion during this study. We greatly appreciate the valuable technical assistance from Carole Boucayrand, Stephanie Levat, Alan Castillo, and Jean-Claude Harrichouri for creating the open system reactors. The authors would like to gratefully acknowledge financial support from the Norwegian Research Council, Norsk Hydro, the Centre de la Recherche Scientifique, and the European Union (Contract No. HPRN-CT-2000-00058).

Literature Cited

(1) Lohuis, J. A. O. Carbon dioxide disposal and sustainable development in The Netherlands. *Energy Convers. Manage.* **1993**, *34*, 815−821.

(2) Bachu, S.; Gunter, W. D.; Perkins, E. H. Aquifer disposal of CO_2: hydrodynamic and mineral trapping. *Energy Convers. Manage.* **1994**, *35*, 269−279.

(3) Gunter, W. D.; Bachu, S.; Law, D. H. S.; Marwaha, V.; Drysdale, D. L.; MacDonald, D. E.; McCann, T. J. Technical and economic feasibility of CO2 disposal in aquifers within the Alberta Sedimentary Basin, Canada. *Energy Convers. Manage.* **1996**, *37*, 1135−1142.

(4) Saylor, B.; Matisoff, G.; Morrison, P. Geologic and geochemical evaluation of the potential for CO_2 disposal in deep saline aquifers beneath Ohio. *Proc., Natl. Conf. Carb. Seq., Washington* **2001**; p 12.

(5) White, S. P.; Allis, R. G.; Moore, J.; Chidsey, T.; Morgan, C.; Gwynn, W.; Adams, M. Injection of CO2 into an unconfined aquifer located beneath the Colorado, Central Utah, USA. *Proc. Annu. Conf. Carb. Seq., Alexandria, VA* **2003**; p 15.

(6) Johnson, J. W.; Nitao, J. J.; Steefel, C. I.; Knauss, K. G. Reactive transport modeling of geologic CO_2 sequestration in saline aquifers: The influence of intra-aquifer shales and the relative effectiveness of structural solubility, and mineral trapping during prograde and retrograde sequestration. *Proc., Natl. Conf. Carb. Seq., Washington* **2001**.

(7) Gaus, I.; Azarounal, M.; Czernichowski-Lauriol, I. Reactive transport modeling of dissolved CO2 in the cap rock base during CO2 sequestration (Sleipner site, North Sea). *Proc. Annu. Conf. Carb. Seq., Alexandria, VA* **2003**.

(8) Xu, T.; Apps, J. A.; Pruess, K. Numerical simulation of CO_2 disposal by mineral trapping in deep aquifers. *Appl. Geochem.* **2004**, *19*, 917−936.

(9) Dyni, J. R. *Sodium carbonate resources at the Green River Formation*; U.S. Geological Survey Open-File Report 96-729; U.S. Department of the Interior: Denver, 1996; p 39.

(10) Baker, J. C.; Bai, G. P.; Hamilton, P. J.; Golding, S. D.; Keene, J. B. Continental-scale magmatic carbon dioxide seepage recorded by Dawsonite in the Bowen Gunnedah-Sydney Basin system, Eastern Australia. *J. Sediment. Res.* **1995**, *A65*, 522−530.

(11) Pearce J. M.; Holloway S.; Wacker H.; Nelis M. K.; Rochelle C.; Bateman K. Natural occurrences as analogues for the geological disposal of carbon dioxide. *Energy Convers. Manage.* **1996**, *37*, 1123−1128.

(12) Parkhurst, D. L.; Appelo, C. A. J. *User's guide to PHREEQC (version 2) − A computer program for speciation, batch-reaction, one-*

dimensional transport, and inverse geochemical calculations. U.S. Geological Survey Water-Resources Investigations Report 99-4259; U.S. Department of the Interior: Denver, 1999; p 312.
(13) Helgeson, H. C. Thermodynamics of hydrothermal systems at elevated temperatures. *Am. J. Sci.* 1969, *267*, 729−804.
(14) Soave, G. Equilibrium constants from a modified Redlich-Kwong equation of state. *Chem. Eng. Sci.* **1972**, *27*, 1197−1203.
(15) Mollerup, J. M.; Michelsen, M. L. Calculation of thermodynamic equilibrium properties. *Fluid Phase Equilibr.* **1992**, *74*, 1−15.
(16) Plummer, L. N.; Wigley, T. M. L. The dissolution of calcite on CO_2-saturated solutions at 25 °C and 1 atm total pressure. *Geochim. Cosmochim. Acta* **1976**, *40*, 191−201.
(17) Sjöberg, E. L. A fundamental equation for calcite dissolution kinetics.*Geochim. Cosmochim. Acta* **1976**, *40,* 441−447.
(18) Busenberg, E.; Plummer, L. N. A comparative study of the dissolution and crystal growth kinetics of calcite and aragonite. *Studies Diagenesis*; U.S. Geological Survey Bulletin; Vol. 1578; U.S. Department of the Interior: Reston, VA, 1986; pp 139−168.
(19) Chou, L. R.; Garrels, M.; Wollast, R. Comparative study of the kinetics and mechanism of dissolution of carbonate minerals. *Chem. Geol.* **1989**, *78*, 269−282.
(20) Pokrovsky O. S.; Schott J. Processes at the magnesium-bearing carbonates/ solution interface. II. kinetics and mechanism of magnesite dissolution. *Geochim. Cosmochim. Acta* **1999**, *63*, 881−897.
(21) Pokrovsky, O. S.; Schott, J. Kinetics and mechanism of dolomite dissolution in neutral to alkaline solutions revisited. *Am. J. Sci.* **2001**, *301*, 597−626.
(22) Cubillas, P.; Köhler, P.; Prieto, P.; Oelkers, E. H. Experimental determination of the dissolution rates of calcite, aragonite and bivalves. *Chem. Geol.* **2004**, *216*, 59−77.
(23) Gautelier, M.; Oelkers, E. H.; Schott, J. An experimental study of dolomite dissolution rates as a function of pH from −0.5 to 5 and temperature from 25 to 80 °C *Chem. Geol.* **1999**, *157*, 13−26.
(24) Alkattan, M.; Oelkers, E. H.; Dandurand, J.-L.; Schott, J. An experimental study of calcite and limestone dissolution rates as a function of pH from −1 to 3 and temperature from 25 to 80 °C. *Chem. Geol.* **1998**, *151*, 199−214.
(25) White, A. F.; Brantley, S. L. The effect of time on the weathering of silicate minerals: why do weathering rates differ in the laboratory and field? *Chem. Geol.* **2003**, *202*, 479−506.
(26) Yang, C.; Brantley, S. L. Diopside and anthophyllite dissolution at 25° and 90 °C and acid pH. *Chem. Geol.* **1998**, *147*, 233−248.
(27) Smith, J. T.; Ehrenberg, S. N. Correlation of carbon dioxide abundance with temperature in clastic hydrocarbon reservoirs: relationship to inorganic chemical equilibrium. *Mar. Petrol. Geology*, **1989**, *6*, 129−135.
(28) Keiffer, B.; Jove, C. F.; Oelkers, E. H.; Schott, J. An experimental study of the reactive surface area of the Fontainebleau sandstone as a function of porosity, permeability, and fluid flow rate. *Geochim. Cosmochim. Acta* **1999**, *63*, 3525−3534.
(29) Tester, J. W.; Worley, G. W.; Robinson, B. A.; Grigsby, C. O.; Feerer, J. L. Correlating quartz dissolution kinetics in pure water from 25 to 625 °C. *Geochim. Cosmochim. Acta,* **1994**, *58,* 2407−2420.
(30) Blum, A. E.; Stillings, L. L. Chemical weathering of feldspars. In *Chemical Weathering Rates of Silicate Minerals*; White, A. F., Brantley, S. L., Eds.; Review of Minerals 31; Mineralogical Society of America: Washington, DC, 1995; pp 291−351.
(31) Nagy, K. L. Dissolution and precipitation kinetics of sheet silicates. In *Chemical Weathering Rates of Silicate Minerals*; White, A. F., Brantley, S. L., Eds.; Review of Minerals 31; Mineralogical Society of America: Washington, DC, 1995; pp 173−233.
(32) Svensson, U.; Dreybrodt, W. Dissolution kinetics of natural calcite minerals in CO_2-water systems approaching calcite equilibrium. *Chem. Geol.* **1992**, *100*, 129−145.

Received for review March 10, 2005. Revised manuscript received June 19, 2005. Accepted June 20, 2005.

ES0504791